Theory of high-order sum and difference frequency mixing in a strong bichromatic laser field

Mette B. Gaarde,[1,2] Anne L'Huillier,[1,3] and Maciej Lewenstein[3]
[1]*Department of Physics, Lund Institute of Technology, S-221 00 Lund, Sweden*
[2]*Niels Bohr Institute, Ørsted Laboratory, 2100 Copenhagen, Denmark*
[3]*Commissariat à l'Energie Atomique, DSM/DRECAM/SPAM, Centre d'Etudes de Saclay, 91191 Gif-sur-Yvette, France*
(Received 19 April 1996)

We generalize the recently formulated theory of high-order harmonic generation by low-frequency laser fields to the case of high-order sum and difference frequency mixing in a two-color field of noncommensurate frequencies in the optical-infrared regime. Our theoretical description includes both the single-atom response and propagation. We observe a different behavior of the sum and difference frequency mixing processes, in the single-atom response as well as in the propagation results. The results of our calculations including propagation compare very well with recent experimental observations. [S1050-2947(96)04109-1]

PACS number(s): 42.50.Hz, 32.80.Rm, 42.65.Ky

I. INTRODUCTION

The interaction between a strong two-color laser field and free atoms has been a subject of increasing interest during the past few years. Mixing processes and harmonic generation in a two-color field have been extensively studied theoretically [1–6] as well as experimentally [7–10]. There are several interesting aspects of two-color mixing: (i) the access to new frequencies, not obtainable by harmonic generation; (ii) the tunability, if one of the fields is tunable [8,10]; (iii) the enhancement of the conversion efficiency for harmonic generation [5–7,9], by up to several orders of magnitude if the second field is as intense as the first one; and (iv) the possibility of controlling the harmonic-generation process with the second color [3]. Control could be obtained both in the single-atom response, via control of the electronic trajectories, and in a macroscopic sense, due to control of phase matching. Previous studies of two-color mixing can be divided into two main categories: those involving a fundamental field and one of its harmonics (second or third) [1,3–7,9], which can be as intense as the fundamental, and with, in some cases, a related, controlled, phase; and those involving an intense fixed-frequency field and a weaker tunable field with a different frequency [1,8,10].

Most of the theoretical calculations have been performed by numerically integrating the Schrödinger equation for a single atom in an intense two-color field, either for a hydrogen atom [5] or for a model potential atom [4]. Telnov *et al.* [6] used a Floquet approach to study hydrogen. Ivanov *et al.* [3] used two fields with very similar frequencies to explore various control aspects of intense-field interactions. Long *et al.* [1] studied different two-color mixing scenarios (with parallel or perpendicular polarizations, commensurate or incommensurate frequencies) using a semianalytical approach valid for a zero-range atomic potential [11], which is closely related to ours [12]. All these calculations, however, consider only the single-atom response. Phase matching for sum and difference frequency mixing processes has been discussed many years ago (see, for example, [13]) and was revisited recently for high-order processes [14,15]. High-order difference frequency mixing is predicted to be more efficient than sum frequency mixing and harmonic generation, since for difference frequency mixing the signs of the phase shifts induced by dispersion and by focusing are opposite, whereas they are equal for sum frequency mixing or harmonic generation.

In a recent Letter [10] we presented an experimental study of high-order sum and difference frequency mixing in the 7–70 eV range, in xenon, argon, and neon. This was done by mixing the light from a femtosecond titanium-sapphire laser and that from an optical parametic generator. We obtained tunable radiation through mixing processes involving absorption or emission of one or two photons from the weak tunable source, up to an energy of 70 eV, thus extending the previous work of Eichmann and co-workers [8]. We also found that the relative strengths of the sum and difference frequency processes change, the sum frequency processes being stronger at low photon energies in xenon and the difference frequency processes dominating at high photon energies in neon, being almost comparable to harmonic generation. One of the main motivations of the present work was to develop a theoretical approach allowing us to interpret such experiments and, more generally, to provide a guide to further experimental two-color studies.

The understanding of physics involved in the generation of high-order harmonics [16–18] has recently made considerable progress, owing to the elaboration of the so-called two-step model [19,20]. In this model, the electron is first released from the nucleus by tunneling ionization and then propagates in the electric field. If it returns to the vicinity of the nucleus, it may recombine and thereby release a photon with energy corresponding to the kinetic energy of the electron plus the ionization potential. The return kinetic energy varies depending on the trajectory the electron follows in the continuum. The maximum energy the electron can acquire in the field is $3.2U_p$ (U_p being the ponderomotive potential of the laser field), which gives rise to the cutoff law for the energy of the highest harmonic: $E_{\max}=I_p+3.2U_p$ [17]. Quantum-mechanical approaches [21,22,12] gave firm grounds to this interpretation and indeed expressed the time-dependent dipole moment (whose Fourier transform gives the harmonic components) as a sum of contributions from the different trajectories of the electron in the continuum. Furthermore, we showed [23] that there are mainly two tra-

jectories contributing to the generation of a particular harmonic in the plateau, both of them with return times within the first period of the laser field (the return time is the time spent by the electron in the continuum). The quantum interference between the two trajectories gives rise to oscillations in the strength, as well as in the phase, of the harmonic, as a function of the laser intensity [23]. For a harmonic in the cutoff region, there is only one dominant trajectory and there are no interference effects. Trajectories with return times longer than one period exist, but do not contribute significantly to the generation process even in the plateau [23]. Another important effect is the rapid variation of the phase of the dipole moment for each harmonic component, with the fundamental intensity. This was found to be extremely important to understanding propagation effects and the coherence properties of the emitted radiation [24,25].

In this paper we present a study of the interaction between free atoms and a two-color field, consisting of a strong infrared laser field and a much weaker (by three orders of magnitude) optical field of variable frequency. We present single-atom data as well as calculations including propagation. For the single-atom response, we generalize the quantum-mechanical two-step approach [12] to the case of a two-color field. We include the second field as a perturbation to the atom and the first field and go to second order in the sense that we allow the second field to contribute one or two photons to the generation process. This approximation is justified because the second field is indeed much weaker than the first one and further motivated by the wish to do a full calculation including propagation. A detailed knowledge of the amplitude and phase of the atomic polarization as a function of the intensities of the driving fields is necessary for propagation calculations. Treating nonperturbatively two laser fields of different colors would require manipulating prohibitively large arrays representing the nonlinear polarization in the medium. We generalize our approach to propagation of harmonic fields to the case of two-color frequency mixing. The propagation equations are solved within the paraxial and slowly varying envelope approximations using the dipole moments—dependent on the laser intensity of the intense field—expanded to second order in the weak field.

We observe a difference between sum and difference frequency mixing. This difference is present already in the single-atom response and is enhanced due to phase matching. It comes from the fact that the addition of even a weak second field influences the generation processes. The two previously mentioned electronic trajectories are modified by the presence of the second field and different interference effects result in different phase response of the two processes.

The paper is organized as follows. We describe the single-atom response in Sec. II and the propagation calculations in Sec. III. Section IV contains numerical results, both single-atom data and calculations including propagation. We also compare successfully our numerical results to experimental data [10]. Finally, in Sec. V we discuss our results and draw some conclusions.

II. SINGLE-ATOM RESPONSE

We consider an atom in the one-electron approximation, submitted to an intense two-color electromagnetic field $E(t)=E_1(t)+E_2(t)=E_1\cos(\omega_1 t)+E_2\cos(\omega_2 t+\phi)$, where both fields are linearly polarized in the x direction, hence also the total field. The two frequencies are noncommensurate, both in the optical regime, and ϕ is the relative phase between the two fields. We consider the case where the field $E_1(t)$ is much stronger than the field $E_2(t)$, with a typical intensity ratio of $E_1^2/E_2^2=10^3$. In the following, we often refer to $E_1(t)$ as the ''first,'' the ''fundamental,'' or the ''strong'' field and to $E_2(t)$ as the ''second'' or ''weak'' field. We closely follow the approach described in detail in [12] and summarize only the first few steps. We make the following basic assumptions.

(i) The ground state of the atom is the only bound state that is considered.

(ii) Depletion of the ground state is neglected.

(iii) As soon as the electron is in the continuum, it is treated as a particle moving freely in the electromagnetic field, i.e., we neglect the influence of the atomic potential.

By solving the time-dependent Schrödinger equation with these simplifications, we obtain the following expression for the time-dependent dipole moment of an atom in a field of arbitrary temporal shape:

$$x(t)=i\int_0^t dt' \int d^3p\, d_x^*[\vec{p}-\vec{A}(t)]\exp[-iS(\vec{p},t,t')] \times E(t')d_x[\vec{p}-\vec{A}(t')]+\text{c.c.}, \quad (1)$$

where $\vec{d}(\vec{p},t)$ is the field-free atomic dipole moment (which depends on the choice of the atomic wave function), $E(t)=E_1(t)+E_2(t)$, with a total vector potential $\vec{A}(t)=[-(E_1/\omega_1)\sin(\omega_1 t)-(E_2/\omega_2)\sin(\omega_2 t+\phi),0,0]$, and

$$S(\vec{p},t,t')=\int_{t'}^{t} dt''\left(\frac{[\vec{p}-\vec{A}(t'')]^2}{2}+I_p\right). \quad (2)$$

We have defined a canonical momentum $\vec{p}$ as $\vec{p}=\vec{v}+\vec{A}(t)$, where $\vec{v}$ characterizes a continuum state of kinetic energy $\vec{v}$. In expression (1) we have neglected the contribution of the continuum-continuum part of the mean atomic dipole moment, which is negligible in the limit of weak depletion of the ground state.

Equation (1) has a straightforward physical interpretation: the term $E(t')d_x[\vec{p}-\vec{A}(t')]$ is the probability amplitude for an electronic transition at time t' from the ground state to the continuum state with canonical momentum $\vec{p}$. The electronic wave function is then propagated from time t' until time t, thereby acquiring a phase factor equal to $\exp[-iS(\vec{p},t,t')]$, where $S(\vec{p},t,t')$ is the quasiclassical action. The last term $d_x^*[\vec{p}-A(t)]$ describes the recombination from the continuum state of (canonical) momentum $\vec{p}$ to the ground state at time t.

The dipole moment is thus determined as a fourfold integral. The integration over $\vec{p}$ can be performed using a saddle-point method since only the stationary points of the classical action will contribute significantly to the integral. The saddle point of the action is found to be

$$p_{\rm st}=\frac{E_1}{\omega_1^2\tau}[\cos(\omega_1 t)-\cos(\omega_1 t')] + \frac{E_2}{\omega_2^2\tau}[\cos(\omega_2 t+\phi)-\cos(\omega_2 t'+\phi)]. \quad (3)$$

Insertion of $p_{\rm st}$ in S yields the stationary point of the action $S_{\rm st}$,

$$\begin{aligned} S_{\rm st}=&[I_p+U_1+U_2]\tau-\frac{2U_1}{\omega_1^2\tau}[1-\cos(\omega_1\tau)] \\ &-\frac{2U_2}{\omega_2^2\tau}[1-\cos(\omega_2\tau)]-\frac{U_1}{\omega_1}C_1(\tau)\cos\left[2\omega_1\left(t-\frac{\tau}{2}\right)\right] \\ &-\frac{U_2}{\omega_2}C_2(\tau)\cos\left[2\omega_2\left(t-\frac{\tau}{2}\right)+2\phi\right] \\ &+4\sqrt{U_1U_2}C_+(\tau)\cos\left[\omega_+\left(t-\frac{\tau}{2}\right)+\phi\right] \\ &-4\sqrt{U_1U_2}C_-(\tau)\cos\left[\omega_-\left(t-\frac{\tau}{2}\right)-\phi\right], \end{aligned} \quad (4)$$

where we have introduced new variables, the return time $\tau=t-t'$, $\omega_+=\omega_1+\omega_2$, and $\omega_-=\omega_1-\omega_2$. U_1 and U_2 are the ponderomotive potentials of the two fields $U_1=E_1^2/4\omega_1^2$ and $U_2=E_2^2/4\omega_2^2$, respectively. Expressions for the (real) functions $C_1(\tau),C_2(\tau),C_+(\tau)$, and $C_-(\tau)$ can be found in Appendix B.

To proceed from this point, one has to specify the field-free atomic dipole moments. For hydrogenlike atoms and transitions from s states, the dipole moment can be approximated by [12,26]

$$\vec{d}(\vec{p})=i\frac{2^{7/2}\alpha^{5/4}}{\pi}\frac{\vec{p}}{(p^2+\alpha)^3}, \quad (5)$$

where $\alpha=2I_p$. Many of the relevant properties of the harmonic spectra and their relative intensities, however, can be reproduced using the much simpler dipole moment $\vec{d}(\vec{p})\propto\vec{p}$ [corresponding to the ''broad Gaussian model'' (GBR) described in [12]]. In particular, the GBR model gives the correct dependences of a given harmonic strength and phase of the laser intensity and the ionization potential and the correct relative phases between different harmonics. It has the tremendous advantage of leading to particularly simple analytical expressions. The GBR model has two drawbacks, however: it overestimates the contribution of the lower-order harmonics and it gives uncorrect relative strengths of the harmonics in the plateau, leading to a plateau increasing slightly with the harmonic number [12].

Inserting $\vec{d}(\vec{p})=i\vec{p}$ into Eq. (1) and performing the integration over $\vec{p}$ gives the following expression for the time-dependent dipole moment:

$$\begin{aligned} x(t)=i\int_0^\infty d\tau\left(\frac{\pi}{\epsilon+i\tau/2}\right)^{3/2}&\exp(-iS_{\rm st})\{E_1\cos[\omega_1(t-\tau)] \\ &+E_2\cos[\omega_2(t-\tau)+\phi]\} \\ \times\Bigg(&2U_1K_1(\tau)+2U_1B_1(\tau)\cos\left[2\omega_1\left(t-\frac{\tau}{2}\right)\right] \\ &+2U_2K_2(\tau)+2U_2B_2(\tau)\cos\left[2\omega_2\left(t-\frac{\tau}{2}\right)+2\phi\right] \\ &+4\sqrt{U_1U_2}\Bigg\{D_+(\tau)\cos\left[\omega_+\left(t-\frac{\tau}{2}\right)+\phi\right] \\ &-D_-(\tau)\cos\left[\omega_-\left(t-\frac{\tau}{2}\right)-\phi\right]\Bigg\}\Bigg)+\text{c.c.} \end{aligned} \quad (6)$$

ϵ is a positive regularization constant. The expressions for the (real) functions $K_i(\tau),B_i(\tau)$, and $D_\pm(\tau)$ can be found in Appendix B. For a different choice of atomic dipole moments, these functions would be different (and might not be real), but the expression in Eq. (6) for the dipole moment $x(t)$ would be the same. Note the characteristic $[\pi/(\epsilon+i\tau/2)]^{3/2}$ factor describing diffusion of the electronic wave packet, which effectively cuts off harmonic generation after a few cycles of the field.

The dipole moment can be evaluated directly from Eq. (6) by inserting the expression for $S_{\rm st}$ and using the fact that $\exp[i\nu\cos(\theta)]$ can be expanded as a series of Bessel functions: $\exp[i\nu\cos(\theta)]=\Sigma_n J_n(\nu)i^n e^{-in\theta}$. Since there are four frequency terms in Eq. (4), namely, $\omega_1,\omega_2,\omega_+$, and ω_-, $x(t)$ becomes a fourfold expansion of Bessel functions and its Fourier transform yields the frequency spectrum. This approach is very close to that of Ref. [1] and is indeed very appealing since it yields (almost) exact numerical solutions, independently of the relative strengths of the two fields. However, it is not well adapted to a propagation calculation because it requires a rather time-consuming fourfold infinite sum of Bessel functions for a two-dimensional grid of intensities (I_1,I_2) of the two fields. Instead, we choose a perturbative approach, in which we utilize the fact that U_2 is small compared to U_1. In the expression for the phase factor $\exp(-iS_{\rm st})$, only the first term in $\cos[2\omega_1(t-\tau/2)]$ is written as a sum of Bessel functions

$$\begin{aligned} &\exp\left\{i\frac{U_1}{\omega_1}C_1(\tau)\cos\left[2\omega_1\left(t-\frac{\tau}{2}\right)\right]\right\} \\ &\quad=\sum_n J_n\left(\frac{U_1}{\omega_1}C_1(\tau)\right)(i)^n e^{in\omega_1\tau}e^{-i2n\omega_1 t}. \end{aligned} \quad (7)$$

The remaining terms, i.e.,

$$\exp\left\{i\frac{U_2}{\omega_2}C_2(\tau)\cos\left[2\omega_2\left(t-\frac{\tau}{2}\right)+2\phi\right]\right\} \quad (8)$$

and

$$\begin{aligned} \exp\Bigg(&-i4\sqrt{U_1U_2}\eta\Bigg\{C_+(\tau)\cos\left[\omega_+\left(t-\frac{\tau}{2}\right)+\phi\right] \\ &-C_-(\tau)\cos\left[\omega_-\left(t-\frac{\tau}{2}\right)-\phi\right]\Bigg\}\Bigg), \end{aligned} \quad (9)$$

are expanded to the second order in E_2, i.e., to the first order in U_2. (We typically use $I_2=10^{11}$ W/cm^2 and $\lambda_2=500$ nm,

which give U_2/ω_2 of the order of 10^{-3}, much smaller than $U_1/\omega_1 \simeq 1$.) This approximation corresponds to allowing the weak field to contribute by one or two photons in emission or absorption to the frequency conversion processes. We insert these expansions into Eq. (6) and obtain a new expression for the dipole moment. We then calculate analytically the Fourier components of $x(t)$ by long, but elementary, algebraic manipulations.

In order to improve our atomic model, we normalize the Fourier components of photon energy E by multiplying them by the factor

$$\frac{2^7 \alpha^{5/2}}{\pi^2} \frac{1}{(2E)^3}. \tag{10}$$

This allows us to introduce, in an approximate way, the energy dependence of the hydrogenic dipole moments [see Eq. (5)], thus obtaining a more correct plateau behavior for harmonic generation. Unfortunately, this normalization overestimates even more than before the strengths of the lower-order harmonics [27]. The results presented below are valid only for sufficiently high-order harmonics, of energy larger than I_p. The expressions for the strengths of the Fourier components of Eq. (6) are given in Appendix A.

III. PROPAGATION

The second step of the theoretical description consists of solving the propagation equations in the paraxial and slowly varying envelope approximations, using the dipole moments discussed above as source terms. The method for solving the propagation equations has been discussed previously [28,29]. Here we generalize it to the case of two-color frequency mixing.

We start from the general wave equation describing the propagation of an electromagnetic field $\vec{\mathcal{E}}(\vec{r},t)$ in an isotropic, globally neutral, nonmagnetic, dielectric medium, characterized by an electronic polarization $\vec{\mathcal{P}}(\vec{r},t)$:

$$\nabla^2 \vec{\mathcal{E}}(\vec{r},t) - \frac{1}{c^2} \frac{\partial^2 \vec{\mathcal{E}}(\vec{r},t)}{\partial t^2} = \frac{1}{\epsilon_0 c^2} \frac{\partial^2 \vec{\mathcal{P}}(\vec{r},t)}{\partial t^2}. \tag{11}$$

As in Refs. [28,29], it is natural to decompose $\vec{\mathcal{E}}(\vec{r},t)$ and $\vec{\mathcal{P}}(\vec{r},t)$ as a sum of different frequency components

$$\vec{\mathcal{E}}(\vec{r},t) = \sum_i \vec{\mathcal{E}}_i(\vec{r},t), \quad \vec{\mathcal{P}}(\vec{r},t) = \sum_i \vec{\mathcal{P}}_i(\vec{r},t), \tag{12}$$

where the index i refers to a given frequency ω_i. In the case of incommensurate frequencies, the wave i can be characterized by two integers q_1, q_2, denoting the net total number of photons absorbed or emitted from each laser field (so that $\omega_i = q_1\omega_1 + q_2\omega_2$). In the case of commensurate frequencies, several processes can lead to the same frequency component. For the sake of generality, we make no assumptions about on the frequencies of the two colors.

$\vec{\mathcal{P}}_i(\vec{r},t)$ can be expressed as

$$\vec{\mathcal{P}}_i(\vec{r},t) = \vec{\mathcal{P}}_i^L(\vec{r},t) + \vec{\mathcal{P}}_i^{\rm NL}(\vec{r},t), \tag{13}$$

where $\vec{\mathcal{P}}_i^L(\vec{r},t)$ denotes the *linear response* at the considered frequency and $\vec{\mathcal{P}}_i^{\rm NL}(\vec{r},t)$ the *nonlinear response*. The linear response term is usually incorporated on the left-hand side of the propagation equation, by introducing the refractive index n_i at frequency ω_i. Owing to the relatively low conversion efficiency for the high-order wave mixing processes, the nonlinear response $\vec{\mathcal{P}}_i^{\rm NL}$ is the polarization induced by the fundamental field only. We introduce the envelope functions $\vec{E}_i$ and $\vec{P}_i^{\rm NL}$

$$\vec{\mathcal{E}}_i(\vec{r},t) = \frac{1}{2}\vec{E}_i(\vec{r},t)e^{i(k_i z - \omega_i t)} + \text{c.c.},$$

$$\vec{\mathcal{P}}_i^{\rm NL}(\vec{r},t) = \frac{1}{2}\sum_{q_1,q_2} \vec{P}_{q_1 q_2}^{\rm NL}(\vec{r},t)e^{i(q_1 k_1 z - q_1\omega_1 t + q_2 k_2 z - q_2\omega_2 t)} + \text{c.c.}, \tag{14}$$

with z denoting the coordinate on the propagation axis, $k_i = n_i\omega_i/c$, and the wave vectors at the generated and fundamental ($i=1,2$) frequencies. Note that we have here explicitly summed over the different processes to express the nonlinear polarization. We now make the paraxial and slowly varying envelope approximations. The wave envelopes are assumed to propagate close to the z axis and to vary slowly in the propagation direction (compared to the wavelength) and in time (compared to the period of the process). After a few manipulations described in textbooks (see, e.g., [30]) and, in particular, making the change of variables $\vec{r} \to \vec{r}$ and $t \to t - z/c$, the propagation equations become

$$\nabla_\perp^2 \vec{E}_i(\vec{r},t) + 2ik_i \frac{\partial \vec{E}_i(\vec{r},t)}{\partial z} = -\frac{\omega_i^2}{\epsilon_0 c^2} \sum_{q_1,q_2} \vec{P}_{q_1 q_2}^{\rm NL}(\vec{r},t)e^{-i\Delta k_{q_1 q_2} z}, \tag{15}$$

where $\Delta k_{q_1 q_2} = k_i - q_1 k_1 - q_2 k_2$ denotes the phase mismatch, which, in principle, depends on the process considered. In the calculations presented below, we neglect any dispersion type of effect from free atoms or electrons. $\nabla_\perp^2$ is the Laplacian operating on the transverse coordinates (x, y). Equation (15) is completely general and describes generation and propagation of any field obtained by mixing of two colors. (The generalization to more than two colors is immediate).

In the problem analyzed in the present paper, the two frequencies are assumed to be incommensurate and the second field is treated nonperturbatively up to second order. Both fields are linearly polarized in the x direction, so that all equations above are actually scalar equations. There are five types of processes, namely, $(2K+1,0)$ (harmonic generation), $(2K,\pm 1)$ (absorption or emission of one photon from the second field), and $(2K+1,\pm 2)$ (absorption or emission of two photons from the second field). Using the notations of Appendix A, we rewrite the dipole moments as

$$X_{2K+1} = Y_{2K+1}^0(I_1) + Y_{2K+1}^1(I_1)E_2^2,$$

$$X_{(2K)\pm 1} = Y_{(2K)\pm 1}(I_1)E_2,$$

$$X_{(2K+1)\pm 2} = Y_{(2K+1)\pm 2}(I_1)E_2^2, \tag{16}$$

where the Y coefficients are calculated for a field of amplitude E_1 (assumed to be real). E_2 can be considered as a (real) parameter. The integration of the propagation equations requires the knowledge of the dipoles emitted by each individual atom in the nonlinear medium, experiencing the fields $E_1(\vec{r},t), E_2(\vec{r},t)$, with phases $\varphi_1(\vec{r},t), \varphi_2(\vec{r},t)$. The amplitude and phase of the two fundamental fields are usually obtained by solving the propagation equation for each of them. In the present work, however, we neglect any perturbation of the fundamental fields as they go through the medium, assuming the two fields to be Gaussian, but with different confocal parameters and pulse durations and not necessarily focused at the same position. $\varphi_i(\vec{r})$ $(i=1,2)$ is then simply equal to the phase of a Gaussian beam. Note that the relative phase ϕ between two fields does not play any role since the two frequencies are incommensurate. This is also seen in Eqs. (A1)–(A3), in which ϕ comes in as a constant phase difference and has no influence on the yields of the harmonics or the mixing processes.

The nonlinear polarization in each point $(\vec{r},t)$ can be written as

$$\begin{aligned} P^{\mathrm{NL}}_{2K+1,0}(\vec{r},t) &= 2\mathcal{N}(\vec{r},t)[Y^0_{2K+1}(I_1) \\ &\quad + Y^1_{2K+1}(I_1)I_2]e^{i(2K+1)\varphi_1}, \\ P^{\mathrm{NL}}_{2K,\pm 1}(\vec{r},t) &= 2\mathcal{N}(\vec{r},t)Y_{(2K)\pm 1}(I_1)\sqrt{I_2}e^{i2K\varphi_1 \pm i\varphi_2}, \\ P^{\mathrm{NL}}_{2K+1,\pm 2}(\vec{r},t) &= 2\mathcal{N}(\vec{r},t)Y_{(2K+1)\pm 2}(I_1)I_2 e^{i(2K+1)\varphi_1 \pm 2i\phi_2}, \end{aligned} \tag{17}$$

where the intensities and phases are local variables and $\mathcal{N}(\vec{r},t)$ is the atomic density. The numerical calculations are then performed in two steps. First, the coefficients Y are calculated for a large grid of intensities (about 1000 values are necessary to describe properly the intensity distribution in the nonlinear medium). The value of the nonlinear polarization (17) in each $(\vec{r},t)$ point is obtained by interpolating the $Y(I_1)$ components and multiplying by the appropriate intensity and phase factors. Then, the propagation equation (15) is solved using a Crank-Nicholson algorithm. The integration is repeated several times spanning the laser pulse duration. Note that in the perturbative approach the knowledge of only four functions Y is necessary so that arrays of dimension 4×1000 are enough to describe the polarization. This is in contrast to a full nonperturbative treatment, in which a propagation calculation would require the knowledge of a very large number of Y's (and the dimension of the arrays describing the polarization would be at least 1000×1000).

IV. NUMERICAL RESULTS

We first present single-atom results, obtained by numerical integration of Eqs. (A1)–(A3). All the calculations are performed for a neonlike atom, with an ionization potential of 21.56 eV. We typically integrate over $\tau = 4\times 2\pi$ (four cycles), with 1000 points per cycle. We use intensities of $I_1 = 2.2\times 10^{14}$ W/cm^2 and $I_2 = 10^{11}$ W/cm^2, at wavelengths of $\lambda_1 = 790$ nm and $\lambda_2 = 500$ nm, unless otherwise stated. These parameters have been chosen to match the parameters in our experiment [10].

The sum (difference) frequency process involving the absorption of $2K$ photons from the intense field and the absorption (emission) of one photon from the weaker field will be referred to as $2K+1$ $(2K-1)$ or, in general, as $+1$ (-1) processes. Likewise, processes involving $2K+1$ photons from the strong field and absorption (emission) of two photons from the weaker field will be referred to as $(2K+1)+2$ $[(2K+1)-2]$ or, in general, $+2$ (-2).

A. Single-atom spectra

In Fig. 1 we plot the strengths of the harmonics of the fundamental field and investigate the effect of adding a weak second field. The abscissa scale is the photon energy of the generated radiation, in units of ω_1, i.e., in this case simply the process order. This convention, to express the photon energy in units of the frequency of the fundamental field, will be used in the following. The curves in solid and dotted lines show the results with and without the second field. For our choice of parameters, the influence of the second field is slightly destructive (the solid line is below the dotted line), but this is not always true. For another choice of wavelength of the second field, the situation might be the opposite.

In Fig. 2 we compare the strengths of the different processes. Figure 2(a) shows the harmonics and the ± 1 processes, while Fig. 2(b) presents the harmonics and the ± 2 processes. Several conclusions can be drawn from the figure. First, the mixing processes exhibit the same plateau and cutoff behavior as the harmonic-generation processes, as well as the same strong scattering of the data, due to quantum interferences between different trajectories of the electron in the continuum [12], as mentioned in the Introduction. Second, the strengths of the ± 1 processes are typically a factor of 10–50 lower than the harmonic strengths and the ± 2 processes are again a few orders of magnitude weaker than the ± 1 processes. These results are within 10% of the results obtained in a nonperturbative calculation using the same

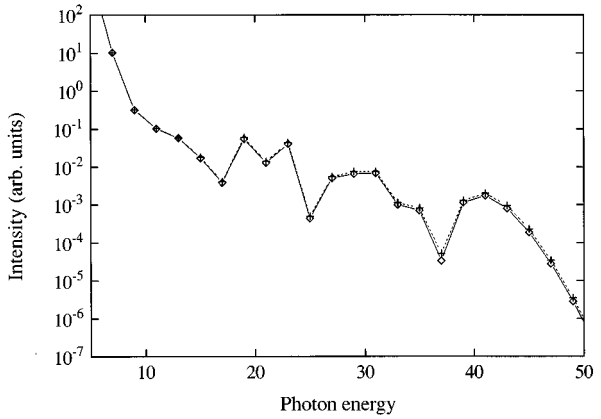

FIG. 1. Strength of harmonics of the strong field when a second weak field is present ($\diamond$) or absent ($+$). The intensities are $I_1 = 2.2\times 10^{14}$ W/cm^2 at $\lambda_1 = 790$ nm and $I_2 = 10^{11}$ W/cm^2 at $\lambda_2 = 500$ nm. The abscissa scale is photon energy, in units of ω_1.

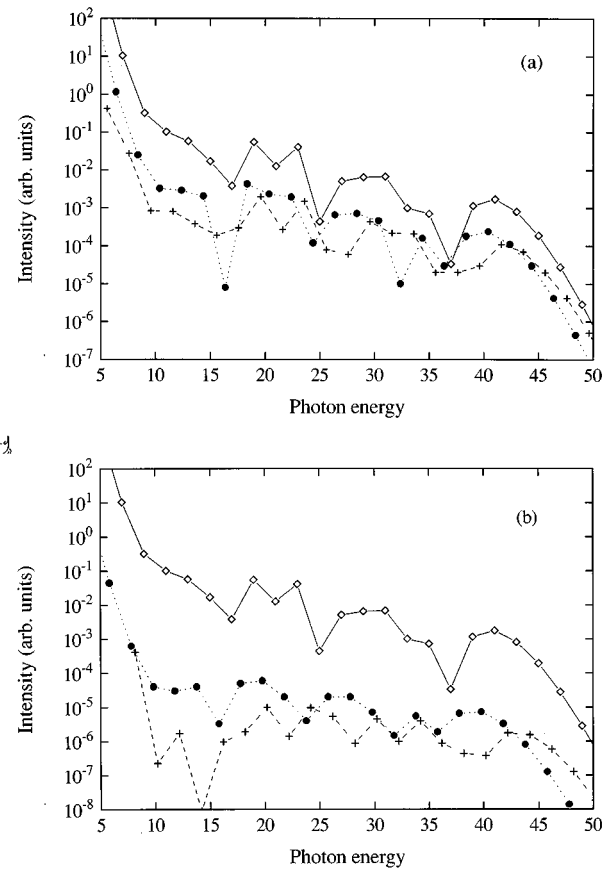

FIG. 2. In (a) we show harmonics ($\diamond$) and processes involving absorption (+) or emission ($\bullet$) of one photon from the weak field and in (b) harmonics ($\diamond$) and processes involving absorption (+) or emission ($\bullet$) of two photons from the second field. The conditions are as in Fig. 1.

atomic model [31]. An increase of the weak field intensity by a factor of 10, i.e., adding a second field a factor of 100 weaker than the first field, yields mixing processes of strength comparable to the harmonic strengths. This is an important consideration since the mixing output could be tunable, in contrast to the harmonics. In this case, however, the perturbative approach is not as good, yielding values about a factor of 2 higher than the nonperturbative calculation. The overall shape of the spectrum and the relative strengths are nevertheless reproduced.

In the cutoff region, there corresponds to each harmonic of energy $(2K+1)\omega_1$ a ''pair'' of -1 and $+1$ frequencies having similar strengths, approximately a factor of 10 lower than the harmonic strength. These are the difference frequency mixing process with energy $(2K+2)\omega_1-\omega_2$ just to the left of the $(2K+1)$th harmonic and the sum frequency mixing process $(2K)\omega_1+\omega_2$ just to the right of the $(2K+1)$th harmonic. Note also the relative strengths of the ± 1 processes, the -1 in general dominating over the $+1$ apart from oscillations due to interference. In the cutoff region, the $+1$ takes over again, becoming comparable in strength to the harmonics. This effect is even more pronounced in Fig. 2(b) for the $+2$ and -2 processes.

The choice to plot the yield of the processes versus photon energy, and not versus process order, has been made for

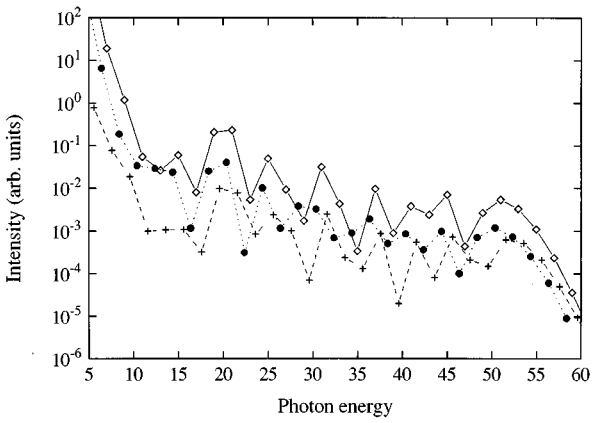

FIG. 3. Strengths of harmonics ($\diamond$) and the $+1$ (+) and -1 ($\bullet$) processes for intensities $I_1=2.2\times10^{14}$ W/cm^2 and $I_2=10^{11}$ W/cm^2.

several reasons. Not only is this a ''spectral'' way of presenting the data and indeed the most convenient for comparison with experimental results, but it is also the most correct in view of the two-step model. Perturbation theory would compare the $2K+1$ and the $2K-1$ processes, which differ in energy by $2\omega_2$. As seen from Fig. 2, this is not an appropriate comparison. Thus we stress that also for the mixing processes it is the *energy* of the returning electron that is important.

In Fig. 3 we investigate the effect of increasing the intensity of the first field to $I_1=3.1\times10^{14}$ W/cm^2 (this is the intensity used later in most of the calculations including propagation). For clarity, we show only the harmonics and the ± 1 processes. The figure shows the extension of the plateau for all of the processes to a cutoff energy of approximatively $55\omega_1$ instead of $45\omega_1$. We again clearly observe a change in the relative strengths of the sum and difference frequency mixing processes depending on the photon energy. Note also that the $+1$ processes are subject to much larger interference effects than the -1 processes.

B. Phase behavior

In Fig. 4 we show the dependence of the dipole phase on the intensity I_1. The solid line corresponds to the 23rd harmonic, the dashed line to the $22+1$ process, and the dot-dashed line to the $24-1$ process (all of these processes lead to approximately the same photon energy). The phase behaviors of the $+1$ and -1 processes are quite different. For low intensities, when the generated spectral component is still in the cutoff region, the mixing and harmonic processes exhibit the same behavior, the phase decreases linearly with the intensity (with a slope of $-3.2U_1$) [23]. However, for an intensity large enough for the harmonic to reach the plateau, which for these mixing processes is approximately 0.75×10^{14} W/cm^2, the phase of the $22+1$ process decreases more rapidly than the one of the $24-1$. Furthermore, the superimposed oscillations due to interferences are more violent for the $22+1$ process than for the $24-1$. At higher intensities, in the plateau region, the phase of both the $22+1$ and the $24-1$ mixing processes decreases as $-6U_p$. The different phase dependences of sum and differ-

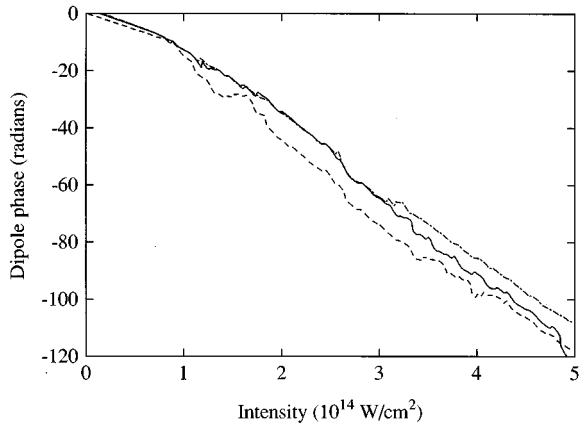

FIG. 4. Phase, in radians, of the 23rd harmonic (solid line) and the $22\omega_1+\omega_2$ (dashed) and the $24\omega_1-\omega_2$ (dot-dashed line) processes as a function of the intensity I_1 of the strong field, in units of 10^{14} W/cm^2.

ence frequency mixing processes are found for all process orders, but the intensity range where the phase behaviors differ changes with the order of the process. Figure 5 shows the phase variations for the $40+1$ and the $42-1$ processes. The steep phase decrease of the $40+1$ is here found at higher intensities, above 4×10^{14} W/cm^2. It is worth mentioning that the $+2$ processes exhibit the same behavior as the $+1$ processes and that the -2 processes behave similarly to the -1 processes.

The phase response of a harmonic dipole moment is usually interpreted in connection with the dominant trajectories responsible for the process. In [23] it was argued that the phase of the dipole is proportional to the return time: $\Phi \propto U_p\tau$. The slope of the phase decrease with intensity is thus interpreted as the return time of the dominant trajectory. For a harmonic in the plateau, there are mainly two trajectories, as previously mentioned, both within the first cycle of the laser field, contributing to the generation process. One has a return time close to half a period, the other has a return time close to one period. It is the latter that dominates the phase response, giving the slope of $-6U_p$. The quantum interference between the two trajectories is responsible for the oscillations superimposed on the phase decrease. In the case of a two-color field, things become more complicated. To interpret the phase behavior, we performed a saddle-point analysis such as the one described in [23]. We found that due to the possibilities of exchanging photons with the second field, there are several processes corresponding to the same electronic trajectory, leading to the same final photon energy. A sum frequency process involving one ω_2 photon corresponds to absorption of one photon from the weak field. This necessarily happens in the vicinity of the nucleus, but can happen either at the time of tunneling or at the time of recombination. Since these two possibilities correspond to the same initial and final states and to the same trajectories, they interfere. Our analysis shows that for the present choice of parameters and in this intensity range the usually dominant trajectory with return time τ_2 close to one period is suppressed in sum frequency generation by destructive quantum interference. On the contrary, this is not the case in difference frequency generation. This leads to an increased relative importance of trajectories with return times close to two or more periods and thus to a faster phase decrease of the $+1$ process [32].

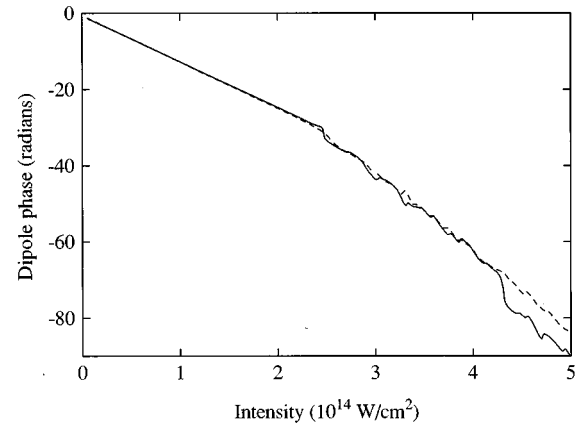

FIG. 5. Phase of the $40\omega_1+\omega_2$ (solid line) and the $42\omega_1-\omega_2$ (dashed line) processes as a function of I_1.

This behavior of the dipole phase plays a very important role when propagation is included, since a large phase variation with intensity deteriorates phase matching. From the above discussion of Figs. 4 and 5, we thus expect propagation to reduce the strength of sum frequency mixing processes, compared to difference frequency mixing, in the high-energy end of the plateau.

C. Results including propagation

In the following, we present calculations including propagation in a gas of neon atoms. The (peak) intensities of the fields are $I_1=3.1\times10^{14}$ W/cm^2 and $I_2=10^{11}$ W/cm^2. The intensity of the strong field was chosen to obtain the same plateau and cutoff energy as in the single-atom case, i.e., slightly higher than before, to account for the reduced cutoff law obtained when propagation is included [21] ($E_{\max}\approx I_p+2U_p$). We let the two beams be Gaussian, with confocal parameters of $b_1=b_2=5$ mm and with the focus at the same position $z_0=0$ in the center of a Lorentzian gas jet with a full width at half maximum of 1.0 mm. The pulse lengths are assumed to be 150 fs. The propagation equations Eq. (15) are integrated on a 1000×300-point grid in $r\times z$ space and in most of the calculations only for one point in time, namely, at the peak intensity. Time integration over the duration of the pulse further smoothes out oscillating structures, but does not change the overall form of the spectra. Ionization due to the fundamental field is omitted in all the calculations, which is not unreasonable at the intensity considered.

In Fig. 6(a) we show the spectra for the $+1$ and the -1 processes. The expected effect of the different intensity dependences of the phase is indeed observed. The difference between the two processes increases in the high-energy end of the plateau. In Fig. 6(b) we show the harmonics and the ±2 processes under the same conditions. In Fig. 7 we show a calculation including integration over 51 points in time. As

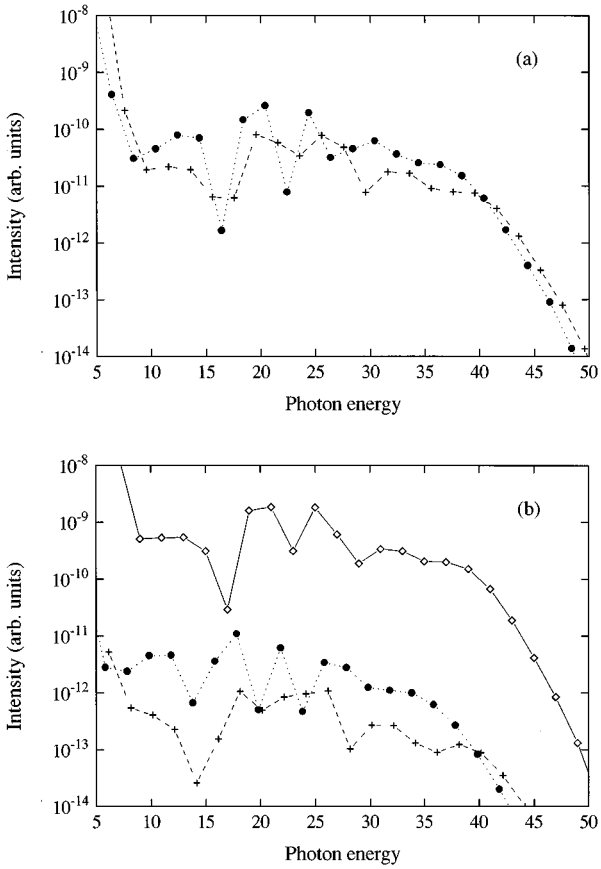

FIG. 6. Spectra, including propagation, for (b) the harmonics ($\diamond$), (a) the $+1$ ($+$) and -1 ($\bullet$) processes, and (b) the $+2$ ($+$) and -2 ($\bullet$) processes. The intensities are $I_1=3.1\times10^{14}$ W/cm^2 and $I_2=10^{11}$ W/cm^2.

mentioned above, this does not change the spectrum dramatically.

To investigate the effect of changing the macroscopic parameters, we translate the focus of the second beam by a value as large as the confocal parameter of the first beam $z_{02}=\pm b_1$ relative to the center of the gas jet. We choose a large confocal parameter of the second beam $b_2=10b_1=50$ mm in order to mimic the experimental conditions of [10] (see Sec. IV D). The result is presented in Fig. 8. The solid lines show the strengths of the ±1 processes when the second focus is before the center of the gas jet and the dotted lines result from a calculation in which the second focus is after the center of the gas jet. All other parameters are as in Fig. 6. We see that the effect is an enhancement of the one process compared to the other, the $+1$ being enhanced when the focus is before the center of the gas jet and the -1 being enhanced when the focus is after the center of the gas jet. It is worth noting that just letting $b_2=10b_1$ and not translating the second focus enhances both the $+1$ and the -1 processes by 20% in the high-energy end of the plateau and in the cutoff, compared to Fig. 6. The results presented in Fig. 8 indicate that the relative strength of the processes depends on the macroscopic parameters and in a nontrivial manner. Moving the focus of the second field by the same distance, on either side of the center of the jet leads to the same relative intensity of the two fields. The effect is, however, clearly asymmetric, reflecting the complex interplay between the geometrical phase and the atomic phase [23]. The overall influence of macroscopic parameters on the relative strengths of the $\pm1,\pm2$ processes remains nevertheless weak. (The vertical scale in Fig. 8 has been deliberately reduced in order to emphasize the effect.) We also investigated the role of the geometrical phase by artificially swapping the geometrical phase factors for sum and difference frequency processes [see Eq. (17)]. The results obtained were very close, much closer than, for example, the difference exhibited by the results corresponding to the two different focus locations in Fig. 8. This shows that the relative shapes of the ±1 spectra are governed essentially by the single-atom response and in particular the intensity dependence of the atomic phase, which itself reflects the dominant trajectories in the single-atom response.

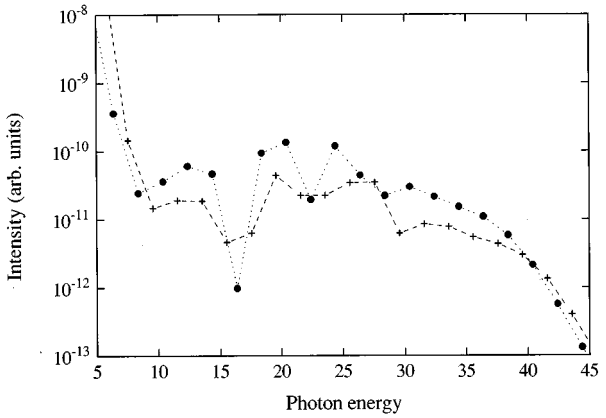

FIG. 7. Identical to Fig. 6(a), with time integration over a 150-fs-FWHM Gaussian laser pulse.

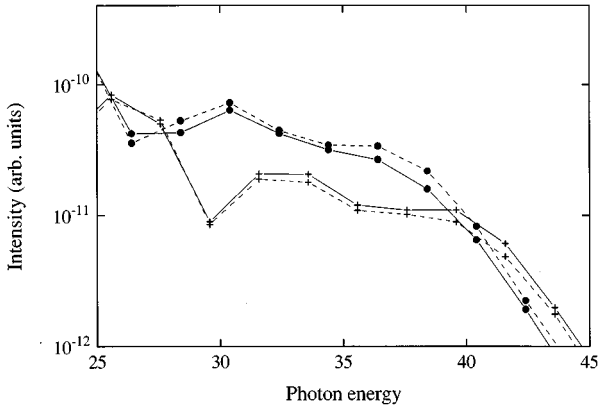

FIG. 8. Effect of changing the relative positions of the two foci, when the confocal parameter of the second field is large ($b_2=10b_1$). Solid lines correspond to a focus at 5 mm before the gas jet ($+$, $+1$ processes; $\bullet$ -1 processes) and dashed lines to a focus 5 mm after the gas jet.

D. Comparison with experimental data

In Figs. 9–11 we compare our numerical simulations to the experimental results of [10], showing the numerical data

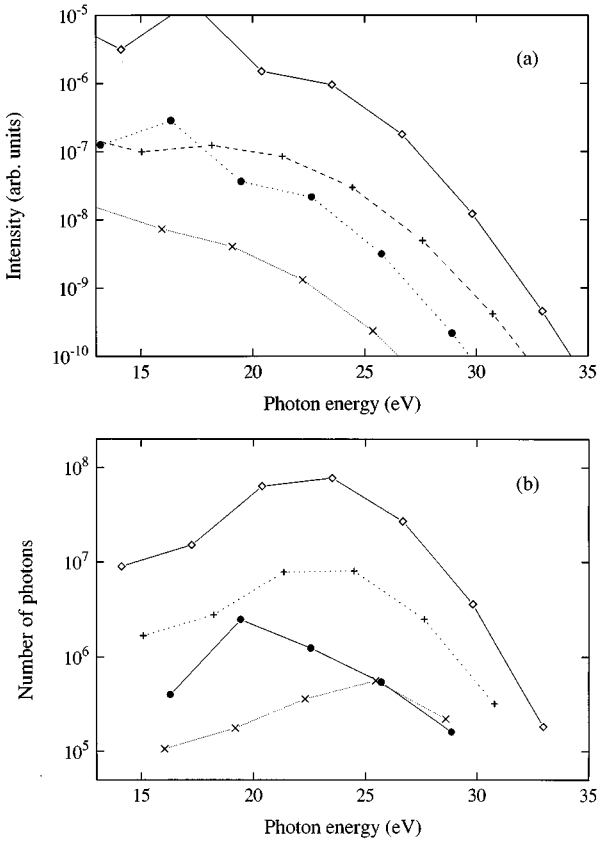

FIG. 9. (a) Calculation including propagation performed in xenon, at intensities of $I_1 = 0.87 \times 10^{14}$ W/cm^2 and $I_2 = 10^{11}$ W/cm^2. The confocal parameter of the second field is 50 mm. We show harmonics ($\diamond$), $+1$ processes ($+$), -1 processes ($\bullet$), and $+2$ processes ($\times$). In (b) we show the experimental result. The abscissa shows the photon energy, in eV.

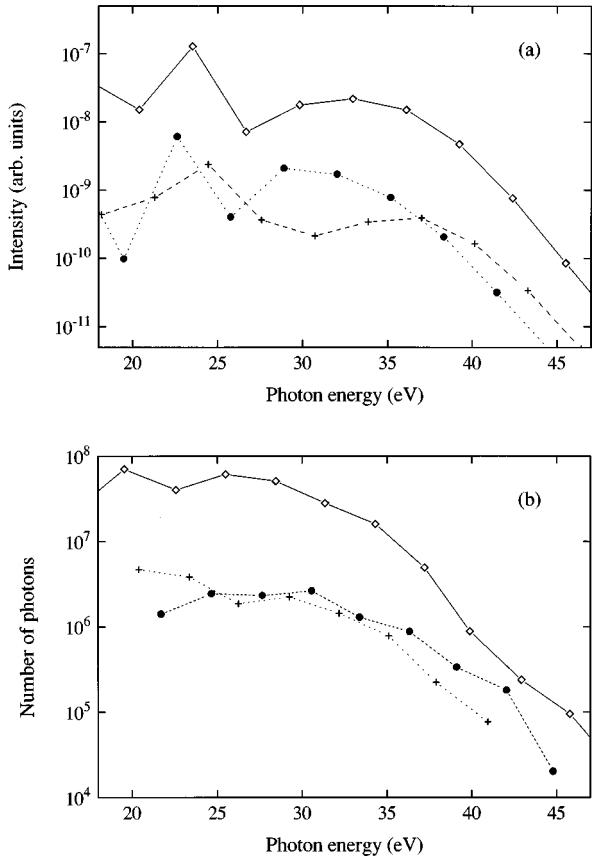

FIG. 10. (a) Calculation in argon, at $I_1 = 1.6 \times 10^{14}$ W/cm^2 and $I_2 = 10^{11}$ W/cm^2. The confocal parameter of the second field is 50 mm. In (b) we show the corresponding experimental result. The notations are as in Fig. 9.

in (a) and the experiments in (b). In all of the three calculations shown in the figures, we have set the confocal parameter of the second field to be $b_2 = 10 b_1 = 50$ mm. Furthermore, we use different intensities of the intense field for the different rare gases, chosen in order to obtain approximately the same cutoff as in the experiment. The intensity of the weak field is kept fixed, as in the experiment. In Fig. 9 we show harmonic generation and mixing processes in xenon ($I_p = 12.13$ eV), at intensities of $I_1 = 0.87 \times 10^{14}$ W/cm^2 and $I_2 = 1 \times 10^{11}$ W/cm^2. The observed dominance of the $+1$ processes over the -1 processes is already present in the single-atom response. This can be interpreted with a dressing picture: Since the photon energy is 2.5 eV, compared to an ionization potential of 12 eV, dressing with plus one photon means an effective I_p of 9.5 eV, compared to an effective I_p of 14.5 eV for difference frequency mixing. Thus sum frequency generation should be favored since it eases the tunneling process. As the phase responses of the $+1$ and -1 processes are similar, phase matching does not change this effect. As Fig. 9(b) shows, the agreement with the experimental results concerning the relative ratios of the processes is satisfying.

Figure 10 shows results for argon ($I_p = 15.76$ eV) at intensities of $I_1 = 1.7 \times 10^{14}$ W/cm^2 and $I_2 = 1 \times 10^{11}$ W/cm^2. The experimental data in Fig. 10(b) show that in argon, the $+1$ and the -1 processes have approximately the same strengths, with -1 processes taking over the $+1$ processes at approximately 25 eV. In the numerical data [Fig. 10(a)] we also see a takeover at $\simeq 25$ eV, but the differences between the strengths of the processes are more pronounced than in the experiment. However, we still consider the agreement to be rather good. Note also that in the cutoff region, the strength of the mixing processes approaches that of the harmonic strength, as was also observed in the experiment.

In Fig. 11 we show the results obtained in neon and the dominance of the -1 processes over the $+1$ processes is clear in both the numerical and the experimental results. In the calculation (see Sec. IV C) we used intensities of $I_1 = 3.1 \times 10^{14}$ W/cm^2 and $I_2 = 1 \times 10^{11}$ W/cm^2. The agreement obtained between numerical and experimental results is excellent.

Figures 10 and 11 show that the yield in the plateau in argon is stronger by three orders of magnitude than the corresponding for neon, in both the simulations and in the experiment. The plateau harmonics in xenon are again a factor of 100 stronger than in argon, in the calculation, which is more than that observed in the experiment.

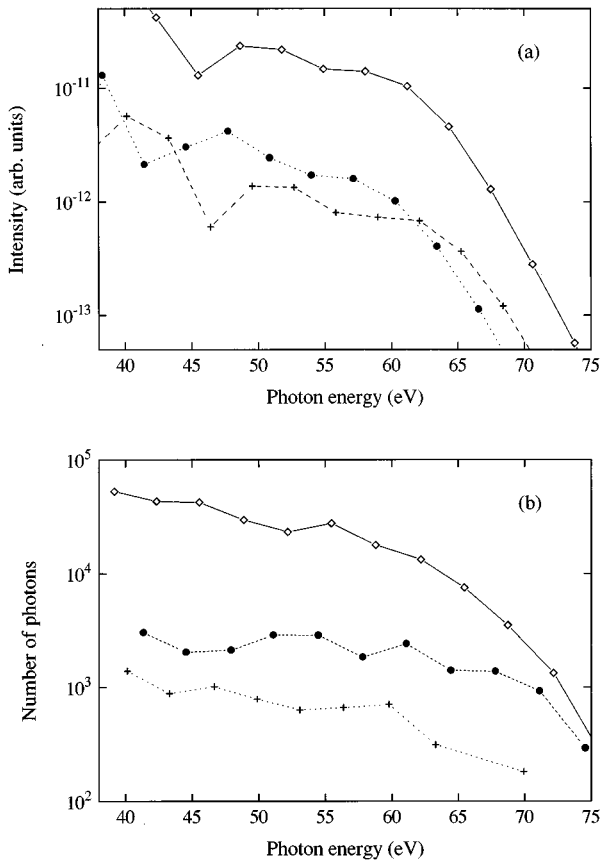

FIG. 11. (a) Calculation in neon, at intensities of $I_1=3.1\times10^{14}$ W/cm^2 and $I_2=10^{11}$ W/cm^2. The confocal parameter of the second field is 50 mm. In (b) we show the experimental result. Notations are as in Fig. 9.

V. DISCUSSION

We presented calculations of the response of free atoms to an intense bichromatic electromagnetic field. We calculated both the response of one-single atom, and the macroscopic response of a collection of atoms to a space- and time-dependent laser pulse. We used a perturbative approximation for the second field. This was motivated by the small relative intensity of the second field (i.e., a factor of 1000 weaker than the fundamental field) and by the wish to perform a propagation calculation.

In the single-atom data, we showed that mixing signals can be obtained with strengths a factor of 10–50 lower than the harmonic strengths. Adding a field this weak does not significantly alter the strengths of the harmonics of the fundamental field. The mixing signals exhibit the same plateau and cutoff behavior as the harmonics. The sum and difference frequency mixing processes exhibit different behaviors. In the spectra, this can be seen as a dominance of $+1$ processes at low photon energies (in xenon) and of -1 processes at higher energies (in neon). Furthermore, the scattering of the $+1$ data with order is more important than that of the -1 data. Moreover, the intensity dependence of the phase is significantly different for the two processes. As an example, we compared the phase dependences of the $22+1$ and the $24-1$ processes and observed that for a certain range of intensity (roughly between 1 and 2×10^{14} W/cm^2), the phase decrease is much steeper for the $22+1$ than for the $24-1$ process, which behaves more or less like a harmonic. We interpreted this difference as a consequence of quantum interferences between different trajectories for the electron in the continuum. Usually, there are two trajectories, with return times within the first laser period, that contribute significantly to the generation of a harmonic. The presence of the second field introduces a number of trajectories leading to the same final energy and these interfere constructively or destructively. For the present choice of parameters, this interference is destructive for the usually dominant trajectory with a return time close to one period for the $+1$ process and not for the -1 process. This allows trajectories with longer return times to contribute more to the generation of the $+1$ processes, which leads to a faster decrease of the phase with the intensity.

When phase matching and propagation are included, this phase behavior enhances the difference between the sum and difference mixing processes. The fast decrease of the dipole phase is observed for the $+1$ processes, at intensities corresponding to the high-energy end of the plateau. Thus phase matching suppresses the $+1$ processes compared to the -1 processes in this range of the plateau. We compared our numerical results to some experimental results and obtained good agreement, in particular in xenon and neon, for the relative strengths of the output signals.

In conclusion, we believe that studies of mixing processes will help to understand, and hence to obtain, control of harmonic generation and its characteristics. We have generalized here the analysis of the harmonic-generation process in terms of quasiclassical trajectories, quantum interferences, and phase-matching effects. This has led to a better understanding of the results, but will also be useful in the search for more efficient generation of harmonics and mixing processes.

Finally, our studies could be easily generalized to different regimes of parameters, such as different polarizations of the two fields, commensurate frequencies, and more than two colors. Particularly interesting is the mixing of the fundamental field with a high-order harmonic beam. This problem has already been studied in the context of coherent control of above-threshold ionization [33]. In our case it could be harmonic generation stimulated by one or several harmonics [34]. More excitingly, our theory could be used to study stimulation of high-order harmonic generation by several harmonics, forming an attosecond pulse train [35].

ACKNOWLEDGMENTS

We thank P. Agostini, Ph. Antoine, W. Becker, B. Carré, P. Lambropoulos, P. Salières, and C.-G. Wahlström for enlighting discussions. We are especially grateful to P. Salières, who has gone through all the analytical expressions. We acknowledge the support of the Swedish Natural Science Research Council. Computer time was provided by the National Supercomputer Centre in Sweden, University of Linköping.

APPENDIX A: FOURIER COMPONENTS OF ATOMIC DIPOLE MOMENT

In this appendix we give the explicit expresssions for the fourier components of the dipole moment. Since we have allowed processes including one and two photons from the weaker field, the atom will radiate at frequencies corresponding to $(2K+1)\omega_1$ (the odd harmonics of the strong laser field), $(2K)\omega_1 \pm \omega_2$, and $(2K+1)\omega_1 \pm 2\omega_2$. First the harmonics of the strong field are

$$
\begin{aligned}
X_{2K+1} = {} & \frac{2i\omega_1 U_1^{3/2}}{[(2K+1)\omega_1]^6}\,\frac{2^7\alpha^{5/2}}{\pi^2}\int_0^\infty d\tau\left(\frac{\pi}{\epsilon+i\tau/2}\right)^{3/2} e^{-iF(\tau)} i^K e^{iK\omega_1\tau}\Bigg\{[-2U_1U_2B_1C_+C_-e^{i\omega_1\tau}]J_{K-2}\left(\frac{U_1}{\omega_1}C_1\right) \\
& + \Bigg[-\frac{i}{2}[1-4U_1U_2(C_+{}^2+C_-{}^2)]B_1e^{i\omega_1\tau} - 2iU_1U_2C_+C_-(2K_1e^{i\omega_1\tau}+B_1) + 2U_2e^{i\omega_1\tau}(C_+D_-+C_-D_+) \\
& - \frac{\omega_2}{\omega_1}U_2B_1(C_+e^{i\omega_-\tau/2} - C_-e^{i\omega_+\tau/2})\Bigg]J_{K-1}\left(\frac{U_1}{\omega_1}C_1\right) + \Bigg[\frac{1}{2}[1-4U_1U_2(C_+{}^2+C_-{}^2)](2K_1e^{i\omega_1\tau}+B_1) + \frac{U_2}{U_1}K_2e^{i\omega_1\tau} \\
& - i\frac{\omega_2}{\omega_1}U_2[C_+e^{i\omega_-\tau/2}(2K_1+B_1e^{i\omega_2\tau}) - C_-e^{i\omega_+\tau/2}(2K_1+B_1e^{-i\omega_2\tau})] - 2iU_2[D_+(2C_+e^{i\omega_1\tau}-C_-) \\
& - D_-(C_+-2C_-e^{i\omega_1\tau})] + 2U_1U_2C_+C_-(2K_1+2B_1e^{i\omega_1\tau}) + \frac{\omega_2U_2}{\omega_1U_1}(e^{i\omega_+\tau/2}D_+ - e^{-i\omega_+\tau/2}D_-)\Bigg]J_K\left(\frac{U_1}{\omega_1}C_1\right) \\
& + \Bigg[\frac{i}{2}[1-4U_1U_2(C_+{}^2+C_-{}^2)](2K_1+B_1e^{i\omega_1\tau}) + i\frac{U_2}{U_1}K_2 + 2iU_1U_2C_+C_-(2K_1e^{i\omega_1\tau}+2B_1) \\
& + i\frac{\omega_2U_2}{\omega_1U_1}(e^{i\omega_+\tau/2}D_+ - e^{i\omega_-\tau/2}D_-) + 2U_2[D_+(2C_+ - C_-e^{i\omega_1\tau}) - D_-(C_+e^{i\omega_1\tau}-2C_-)] \\
& - \frac{\omega_2}{\omega_1}U_2[C_-e^{i\omega_+\tau/2}(2K_1e^{-i\omega_2\tau}+B_1) - C_+e^{i\omega_-\tau/2}(2K_1e^{i\omega_2\tau}+B_1)]\Bigg]J_{K+1}\left(\frac{U_1}{\omega_1}C_1\right) \\
& + \Bigg[-\frac{1}{2}[1-4U_1U_2(C_+{}^2+C_-{}^2)]B_1 - 2U_1U_2C_+C_-(2K_1+B_1e^{i\omega_1\tau}) \\
& + i\frac{\omega_2}{\omega_1}U_2B_1(C_+e^{i\omega_+\tau/2} - C_-e^{i\omega_-\tau/2}) - 2iU_2(C_+D_-+C_-D_+)\Bigg]J_{K+2}\left(\frac{U_1}{\omega_1}C_1\right) \\
& + [-2iU_1U_2C_+C_-B_1]J_{K+3}\left(\frac{U_1}{\omega_1}C_1\right)\Bigg\}. \qquad \text{(A1)}
\end{aligned}
$$

In this expression, we have omitted all arguments τ, e.g., we have written $C_+(\tau)$ as C_+. Expressions for the functions $B_i(\tau), C_i(\tau), D_i(\tau), K_i(\tau)$, and $F(\tau)$ can be found in Appendix B.

For the processes involving absorption or emission of one photon, the Fourier components are [with the label $(2K)\pm 1$ since they include $2K$ photons from the strong field and absorption or emission of one photon from the weak field]

$$
\begin{aligned}
X_{(2K)\pm 1} = {} & \frac{2i\omega_1}{[(2K)\omega_1 \pm \omega_2]^6}\,\frac{2^7\alpha^{5/2}}{\pi^2}U_1\sqrt{U_2}\int_0^\infty d\tau\left(\frac{\pi}{\epsilon+i\tau/2}\right)^{3/2} e^{-iF(\tau)} i^K e^{iK\omega_1\tau} e^{\mp i\phi} e^{-i\omega_\mp\tau/2} \\
& \times\Bigg\{[\pm iU_1B_1C_\pm e^{i\omega_1\tau}]J_{K-2}\left(\frac{U_1}{\omega_1}C_1\right) \\
& + \Bigg[\mp iD_\pm e^{i\omega_1\tau} - \frac{i}{2}\frac{\omega_2}{\omega_1}B_1e^{i\omega_\pm\tau/2} \pm U_1B_1C_\mp e^{i\omega_1\tau} \mp U_1C_\pm(2K_1e^{i\omega_1\tau}+B_1)\Bigg]J_{K-1}\left(\frac{U_1}{\omega_1}C_1\right) \\
& + \Bigg[(\pm D_\pm \mp D_\mp e^{i\omega_1\tau}) + \frac{\omega_2}{\omega_1}K_1e^{i\omega_\pm\tau/2} \mp iU_1[C_\pm(2K_1+B_1e^{i\omega_1\tau}) - C_\mp(2K_1e^{i\omega_1\tau}+B_1)]\Bigg]J_K\left(\frac{U_1}{\omega_1}C_1\right) \\
& + \Bigg[\mp iD_\mp + \frac{i}{2}\frac{\omega_2}{\omega_1}B_1e^{i\omega_\pm\tau/2} \pm U_1[C_\pm B_1 - C_\mp(2K_1+B_1e^{i\omega_1\tau})]\Bigg]J_{K+1}\left(\frac{U_1}{\omega_1}C_1\right) \\
& + [\mp iU_1B_1C_\mp]J_{K+2}\left(\frac{U_1}{\omega_1}C_1\right)\Bigg\}. \qquad \text{(A2)}
\end{aligned}
$$

Finally, the dipole moments for the processes involving absorption or emission of two photons from the weak field are

$$X_{(2K+1)\pm 2}=\frac{2i\omega_1}{[(2K+1)\omega_1\pm 2\omega_2]^6}\frac{2^7\alpha^{5/2}}{\pi^2}\sqrt{U_1}U_2\int_0^\infty d\tau\left(\frac{\pi}{\epsilon+i\tau/2}\right)^{3/2}e^{-iF(\tau)}i^K e^{iK\omega_1\tau}e^{\mp i2\phi}e^{\pm i\omega_2\tau}$$

$$\times\left\{[U_1{}^2B_1C_\pm{}^2e^{i\omega_1\tau}]J_{K-2}\left(\frac{U_1}{\omega_1}C_1\right)+\left[-2U_1C_\pm D_\pm e^{i\omega_1\tau}+iU_1{}^2C_\pm{}^2(2K_1e^{i\omega_1\tau}+B_1)-2iU_1{}^2B_1C_+C_-e^{i\omega_1\tau}\right.\right.$$

$$\left.\mp\frac{\omega_2}{\omega_1}U_1B_1C_\pm e^{i\omega_\pm\tau/2}+\frac{U_1}{4\omega_2}B_1C_2e^{i\omega_1\tau}\right]J_{K-1}\left(\frac{U_1}{\omega_1}C_1\right)$$

$$+\left[\frac{1}{2}B_2e^{i\omega_1\tau}\pm\frac{\omega_2}{\omega_1}D_\pm e^{i\omega_\pm\tau/2}\pm i\frac{\omega_2}{\omega_1}U_1e^{i\omega_\pm\tau/2}(B_1C_\mp-2K_1C_\pm)+2iU_1C_\pm(D_\mp e^{i\omega_1\tau}-D_\pm)\right.$$

$$+2iU_1C_\mp D_\pm e^{i\omega_1\tau}+2U_1{}^2C_+C_-(2K_1e^{i\omega_1\tau}+B_1)+i\frac{U_1}{4\omega_2}C_2(2K_1e^{i\omega_1\tau}+B_1)$$

$$\left.-U_1{}^2(C_\pm{}^2(2K_1+B_1e^{i\omega_1\tau})+C_\mp{}^2B_1e^{i\omega_1\tau})\right]J_K\left(\frac{U_1}{\omega_1}C_1\right)$$

$$+\left[\frac{i}{2}B_2\mp i\frac{\omega_2}{\omega_1}D_\pm e^{-i\omega_\mp\tau/2}-iU_1{}^2[C_\mp{}^2(2K_1e^{i\omega_1\tau}+B_1)+C_\pm{}^2B_1]+2U_1[C_\mp(D_\mp e^{i\omega_1\tau}-D_\pm)-C_\pm D_\mp]\right.$$

$$\left.+2iU_1{}^2C_+C_-(2K_1+B_1e^{i\omega_1\tau})-\frac{U_1}{4\omega_2}C_2(2K_1+B_1e^{i\omega_1\tau})\pm U_1\frac{\omega_2}{\omega_1}e^{i\omega_\pm\tau/2}(B_1C_\pm-2K_1C_\mp)\right]J_{K+1}\left(\frac{U_1}{\omega_1}C_1\right)$$

$$+\left[2iU_1C_\mp D_\mp+U_1{}^2C_\mp{}^2(2K_1+B_1e^{i\omega_1\tau})-2U_1{}^2C_+C_-B_1\mp iU_1\frac{\omega_2}{\omega_1}B_1C_\mp e^{i\omega_\pm\frac{\tau}{2}}-i\frac{U_1}{4\omega_2}C_2B_1\right]J_{K+2}\left(\frac{U_1}{\omega_1}C_1\right)$$

$$+[+iU_1{}^2B_1C_\mp{}^2]J_{K+3}\left(\frac{U_1}{\omega_1}C_1\right)\Bigg\}. \tag{A3}$$

APPENDIX B: ADDITIONAL DEFINITIONS

In this appendix we present the explicit expressions for the functions $C_i(\tau)$, $B_i(\tau)$, $D_i(\tau)$, and $F(\tau)$ that enter the expressions (4) and (6). First, the functions of τ used in Eq. (4) for the stationary point of the action are, for $i=1,2$,

$$C_i(\tau)=\sin(\omega_i\tau)-\frac{4}{\omega_i\tau}\sin^2\left(\frac{\omega_i\tau}{2}\right), \tag{B1}$$

$$C_\pm(\tau)=-\frac{1}{\omega_\pm}\sin\left(\frac{\omega_\pm\tau}{2}\right)-\frac{1}{\omega_1\omega_2\tau}\left[\cos\left(\frac{\omega_+\tau}{2}\right)-\cos\left(\frac{\omega_-\tau}{2}\right)\right]. \tag{B2}$$

Then the functions of τ determined by the choice of the field-free atomic dipole moments are, for $i=1,2$

$$K_i(\tau)=\frac{4}{\omega_i{}^2\tau^2}\sin^2\left(\frac{\omega_i\tau}{2}\right)-\frac{2}{\omega_i\tau}\sin(\omega_i\tau)+\cos(\omega_i\tau), \tag{B3}$$

$$B_i(\tau)=-\frac{4}{\omega_i{}^2\tau^2}\sin^2\left(\frac{\omega_i\tau}{2}\right)+\frac{2}{\omega_i\tau}\sin(\omega_i\tau)-1, \tag{B4}$$

$$D_\pm(\tau)=-\cos\left(\frac{\omega_\mp\tau}{2}\right)-\frac{4}{\omega_1\omega_2\tau^2}\sin\left(\frac{\omega_1\tau}{2}\right)\sin\left(\frac{\omega_2\tau}{2}\right)+\frac{2}{\tau}\left[\frac{1}{\omega_2}\cos\left(\frac{\omega_1\tau}{2}\right)\sin\left(\frac{\omega_2\tau}{2}\right)+\frac{1}{\omega_1}\sin\left(\frac{\omega_1\tau}{2}\right)\cos\left(\frac{\omega_2\tau}{2}\right)\right]. \tag{B5}$$

Finally, the function $F(\tau)$ in Eqs. (A1)–(A3) is

$$F(\tau)=(I_p+U_1+U_2)\tau-\frac{2U_1}{\omega_1^2\tau}[1-\cos(\omega_1\tau)]-\frac{2U_2}{\omega_2^2\tau}[1-\cos(\omega_2\tau)]. \tag{B6}$$

[1] S. Long, W. Becker, and J. K. McIver, Phys. Rev. A **52**, 2262 (1995); see also K. Kondo *et al.*, J. Opt. Soc. Am. B **13**, 424 (1996).
[2] H. Eichmann, A. Egbert, S. Nolte, C. Momma, B. Wellegehausen, W. Becker, S. Long, and J. K. McIver, Phys. Rev. A **51**, R3414 (1995).
[3] M. Yu. Ivanov, P. B. Corkum, T. Zuo, and A. Bandrauk, Phys. Rev. Lett. **74**, 2933 (1995).
[4] M. Protopapas, P. L. Knight, and K. Burnett, Phys. Rev. A **49**, 1945 (1994).
[5] M. Protopapas, A. Sanpera, K. Burnett, and P. L. Knight, Phys. Rev. A **52**, R2527 (1995).
[6] D. M. Telnov, J. Wang, and S.-I Chu, Phys. Rev. A **52**, 3988 (1995).
[7] M. D. Perry and J. K. Crane, Phys. Rev. A **48**, R4051 (1993).
[8] H. Eichmann, S. Meyer, K. Riepl, C. Momma, and B. Wellegehausen, Phys. Rev. A **50**, R2834 (1994).
[9] S. Watanabe, K. Kondo, Y. Nabekawa, A. Sagisaka, and Y. Koboyashi, Phys. Rev. Lett. **73**, 2692 (1994).
[10] M. B. Gaarde, P. Antoine, A. Persson, B. Carré, A. L'Huillier, and C.-G. Wahlström, J. Phys. B **29**, L163 (1996).
[11] W. Becker, S. Long, and J. K. McIver, Phys. Rev. A **50**, 1540 (1995), and references therein.
[12] M. Lewenstein, Ph. Balcou, M. Yu. Ivanov, Anne L'Huillier, and P. Corkum, Phys. Rev. A **49**, 2117 (1994).
[13] G. C. Bjorklund, IEEE J. Quantum Electron. **QE-11**, 287 (1975).
[14] P. L. Shkolnikov, A. E. Kaplan, and A. Lago, Opt. Lett. **18**, 1700 (1993).
[15] P. L. Shkolnikov, A. E. Kaplan, and A. Lago (unpublished).
[16] J. J. Macklin, J. D. Kmetec, and C. L. Gordon III, Phys. Rev. Lett. **70**, 766 (1993); A. L'Huillier and Ph. Balcou, *ibid.* **70**, 774 (1993).
[17] J. L. Krause, K. J. Schafer, and K. C. Kulander, Phys. Rev. Lett. **68**, 3535 (1992).
[18] K. J. Schafer, B. Yang, L. F. DiMauro, and K. C. Kulander, Phys. Rev. Lett. **70**, 1599 (1993).
[19] P. B. Corkum, Phys. Rev. Lett. **73**, 1995 (1993).
[20] K. C. Kulander, K. J. Schafer, and J. L. Krause, in *Super-Intense Laser-Atom Physics*, Vol. 316 of *NATO Advanced Study Institute, Series B: Physics*, edited by B. Piraux, Anne L'Huillier, and K. Rzążewski (Plenum, New York, 1993), p. 95.
[21] A. L'Huillier, M. Lewenstein, P. Salières, Ph. Balcou, M. Yu. Ivanov, J. Larsson, and C.-G. Wahlström, Phys. Rev. A **48**, R3433 (1993).
[22] W. Becker *et al.*, Phys. Rev. A **50**, 1540 (1995), and references therein.
[23] M. Lewenstein, P. Salières, and A. L'Huillier, Phys. Rev. A **52**, 4747 (1995).
[24] The role of the intensity-dependent induced atomic phase has been addressed in several papers: Macklin *et al.* notice it in Ref. [16]; Rae *et al.* discuss the related delay between the maxima of the fundamental field and the maxima of the harmonic emission [S. C. Rae, K. Burnett, and J. Cooper, Phys. Rev. A **50**, 3438 (1994)]; the influence of the phase on the angular distribution of harmonics is discussed by J. E. Muffet, C.-G. Wahlström, and M. H. R. Hutchinson, J. Phys. B **27**, 5693 (1994); and J. Peatross, M. V. Fedorov, and K. C. Kulander, J. Opt. Soc. Am. B **12**, 863 (1995); the influence of the phase on temporal and spectral properties of the harmonics is presented in C. Kan, C. Capjack, R. Rankin, and N. H. Burnett, Phys. Rev. A **52**, R4336 (1995).
[25] P. Salières, A. L'Huillier, and M. Lewenstein, Phys. Rev. Lett. **75**, 3376 (1995).
[26] H. A. Bethe and E. E. Salpeter, *Quantum Mechanics of One and Two Electron Atoms* (Academic, New York, 1957).
[27] This problem has been pointed out to us by P. Lambropoulos. A direct comparison of the harmonic spectra obtained from the exact numerical solutions of the Schrödinger equation and the GBR model shows reasonable agreement deep in the plateau and disagreement for lower harmonics, consisting in a too rapid decrease of the spectra; see E. Cormier and P. Lambropoulos (unpublished).
[28] A. L'Huillier, Ph. Balcou, S. Candel, K. J. Schafer, and K. C. Kulander, Phys. Rev. A **46**, 2778 (1992).
[29] Ph. Antoine, A. L'Huillier, M. Lewenstein, P. Salières, and B. Carré, Phys. Rev. A **53**, 1725 (1995).
[30] Y. R. Shen, *The Principles of Nonlinear Optics* (Wiley, New York, 1984).
[31] Ph. Antoine (private communication).
[32] M. B. Gaarde, Lic. thesis, Lund Institute of Technology, 1996 (unpublished).
[33] V. Véniard, R. Taïeb, and A. Maquet, Phys. Rev. Lett. **74**, 4161 (1995); Phys. Rev. A **54**, 721 (1996).
[34] D. F. Zaretzkii and E. A. Nersesov, Zh. Éksp. Teor. Fiz. **107**, 79 (1995) [JETP **80**, 41 (1995)].
[35] Ph. Antoine, A. L'Huillier, and M. Lewenstein (unpublished).